Anatomical Landmark Based Registration of Contrast Enhanced T1-Weighted MR Images

Ali Demir[1], Gozde Unal[1,⋆], and Kutlay Karaman[2]

[1] Sabanci University, Istanbul, Turkey
ademir@sabanciuniv.edu, gozdeunal@sabanciuniv.edu
[2] Anadolu Medical Center, Kocaeli, Turkey

Abstract. In many problems involving multiple image analysis, an image registration step is required. One such problem appears in brain tumor imaging, where baseline and follow-up image volumes from a tumor patient are often to-be compared. Nature of the registration for a change detection problem in brain tumor growth analysis is usually rigid or affine. Contrast enhanced T1-weighted MR images are widely used in clinical practice for monitoring brain tumors. Over this modality, contours of the active tumor cells and whole tumor borders and margins are visually enhanced. In this study, a new technique to register serial contrast enhanced T1 weighted MR images is presented. The proposed fully-automated method is based on five anatomical landmarks: eye balls, nose, confluence of sagittal sinus, and apex of superior sagittal sinus. After extraction of anatomical landmarks from fixed and moving volumes, an affine transformation is estimated by minimizing the sum of squared distances between the landmark coordinates. Final result is refined with a surface registration, which is based on head masks confined to the surface of the scalp, as well as to a plane constructed from three of the extracted features. The overall registration is not intensity based, and it depends only on the invariant structures. Validation studies using both synthetically transformed MRI data, and real MRI scans, which included several markers over the head of the patient were performed. In addition, comparison studies against manual landmarks marked by a radiologist, as well as against the results obtained from a typical mutual information based method were carried out to demonstrate the effectiveness of the proposed method.

1 Introduction

Image registration refers to the problem of finding a geometric transformation, which is optimal in a certain sense, between two or more corresponding images. Nature of the correspondence problem describes the type of necessary geometric transformation [1]. Registration is a major problem in many medical imaging applications such as image guided neurosurgery, surgical planning, radiotherapy planning, patient population analysis, and monitoring tumor growth.

⋆ This work was partially supported by Tubitak Grant No:108E126, and EU FP7 Grant No: PIRG03-GA-2008-231052.

In this study we focused on the registration of serial Magnetic Resonance (MR) images intended for the change detection problem in tumor monitoring [5,6]. General methods and strategies for image registration are reviewed in [2,3,4]. Registration problem for change detection in brain can be classified as a rigid body motion of invariant brain structures. Therefore, the most challenging part of the change detection is to overlay invariant structures accurately. Ettinger et al. used intracranial cavity (ICC) as an invariant structure to register serial images. Their strategy involves computation of dense point correspondences based on segmented ICC [7]. Anatomical landmark localization on Talairach space is also a popular approach for registration [13,15,14]. Chui et al. extracted the outer cortical surface and major sulcal ribbons to register brain MR images [8]. Geometrical features such as curves, lines, curvatures, corners, and so on, are also used extensively in image registration problems. Davatzikos et al. uses the curves and boundaries in regions to preregister the volumes for elastic registration [9,10]. Geometric landmarks make the registration procedure automatic and robust [11,12,16]. On the other hand, intensity similarity based methods are also widely utilized in most of the registration problems [17,18,19]. Duffau et al. [5] in their review, reported that the image intensity is not a reliable measure in the presence of growing tumors, which introduce additional challenges for registration algorithms. Therefore, detection of invariant landmarks in serial images is expected to perform better than an intensity similarity based optimization approach.

Registration is inherently an ill-posed problem, therefore usually no unique solution is available. Often, constraints are introduced, particularly for a deformable registration problem, constraints on a deformation field can be defined. On the other hand, depending on the domain and application of the problem, specific intensity similarity measures or different feature-based approaches are proposed [1]. In this paper, for the clinical problem of brain tumor monitoring, where anatomical features can be extracted from the contrast enhanced T1-weighted MRI (contrast T1-MRI), we present a new method where strong anatomical features drive the registration without depending on intensity similarity measures, which can become problematic in presence of significant tumor change over time [5]. Another advantage of this approach is that it is invariant due to an intra-patient registration scenario, i.e. the same anatomical landmarks can be found in the follow-up images. Following a first anatomic landmark based registration, an extracted surface, which is constrained by the available anatomical landmarks obtained in the first phase of the method, drives the second phase of the registration. This is a surface registration step that propagates the solution towards matching of the important features over a consistent part of the scalp for a better and extensive fit over the head surface for a refinement of the final affine transformation. Apart from its use in tumor follow-up studies, the proposed rigid/affine registration method can be used as a pre-processing before generic deformable registration applications, which require an initial rigid alignment phase.

The organization of the paper is as follows. In Section 2, the specific anatomical landmarks used in our algorithm and their extraction is described. The proposed registration method based on anatomical landmarks is presented in Section 3. The results are demonstrated in Section 4 with consistency tests and validation studies, followed by conclusion and discussion in Section 5.

2 Extraction of Anatomical Landmarks

The first step of the proposed registration algorithm involves extraction of anatomical brain landmarks on given contrast T1-MRI volumes. Thus, a patient-specific coordinate system, which can be invariably found on all human brain images, is obtained based on five selected anatomical landmarks: nasal bone tip, center of two eyeballs, confluence of sinus, and apex of superior sagittal sinus. The landmark selection process, i.e. determining brain landmarks that can be reliably observed and computationally extracted, was carried out jointly with the radiologists in the team.

2.1 Nasal Bone from Nose

The anatomic landmark extraction step starts with detection of a binary head mask. It is obtained on dilated canny edge map through region growing seeded from the outside at the grid boundaries. This connects the boundary components and complement of this result is eroded with the same size of dilation mask, forming the head mask. Anterior tip point of each axial slice is the nearest point of mask to the top most row of the slice. It is detected with a linear search in rows starting from the top most row. Another geometric definition derived from head mask is the symmetry line estimate which is defined as the line passing through the anterior tip point and center of mass (1^{st} order image moments) of the slice. Noting that this is not necessarily symmetry line of brain, it will be defined after the nose tip points are located. Figure 1-a depicts four geometric

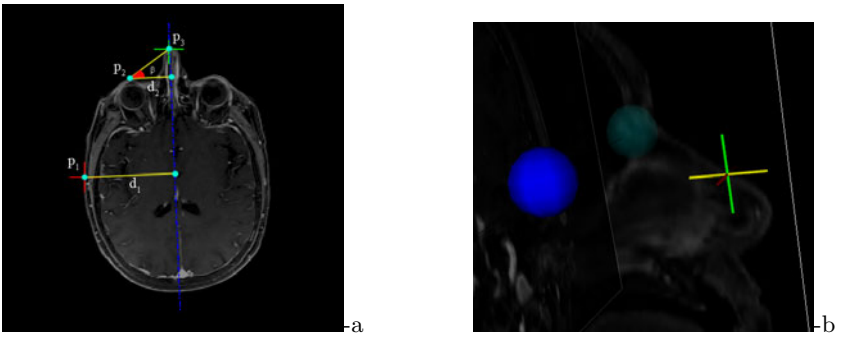

Fig. 1. a)Geometric features (Symmetry line, p_1, p_2, p_3,d_1, and d_2, and the angle β) used to find the nose tip points. b)Detected nose landmark.

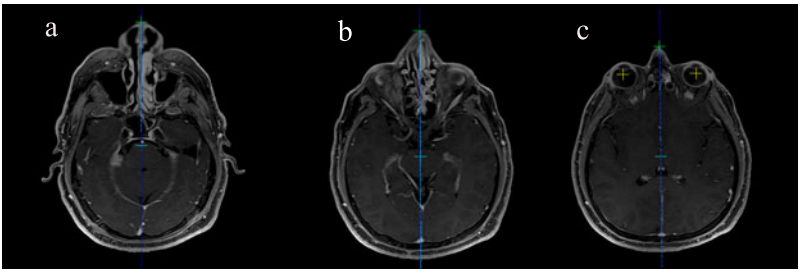

Fig. 2. Sample slices with nose tip points detected: (a) Bottom nose slice, (b) Middle nose slice, c) Top nose slice

features utilized in finding the nasal bone anatomic feature: p_1, the point with the maximum distance to the symmetry line, p_2, the most anterior point of eye balls, and d_1 and d_2 are minimum distances from p_1 and p_2, to the symmetry line. The ratio of $d_2/d_1 := c$ is found to be almost biometric constant with a mean and variance 0.42 ± 0.01, which was measured over 20 MRI scans. Using this constant, for each slice we find p_1 and d_1, then estimate the point p_2, where $d_2 = cd_1$. We also define the angle β between lines of p_2 to anterior tip point (p_3) and p_2 to the corresponding point on symmetry line. Tip points of the slices with high values of $\tan \beta$ are marked as nose tip points. Figure 2 depicts a few sample slices with nose tip points marked. Finally, a single nose landmark is marked at the center of selected nose tip points, which is located at the end point of nasal bone (see Figure 1-b).

2.2 Eye Balls

An eye ball is segmented using a sphere model, which is initiated at a seed point based on the nose feature. Two seed coordinates for the left and right eye balls are first estimated on the top most slice of the nose, e.g. see Figure 2-c, then given d_1, the maximum distance to symmetry axis, d_2 is calculated using the ratio c (Section 2.1). Using an anatomical fact that an eyeball is roughly 10 mm in radius, the seed is initialized 10 mm away from p_2 towards the symmetry

Fig. 3. (a) A slice from the obtained 3D binary eyeball masks; (b) T1-MRI slice marked with estimated seed points on eyeballs

axis to ensure that the seed point falls in the eye ball region. Initialized sphere parameters, the center and the radius, are evolved until convergence with ordinary differential equations derived to maximize the difference between the mean intensity statistics inside and outside the sphere within a band around its surface. A sample slice from 3D eye mask and estimated eyeball seeds are shown in Figure 3.

2.3 Confluence of Sinus

Confluence of sinus is the conjunction point of the superior sagittal sinus, straight sinus, and occipital sinus. A distinguishing feature of the confluence of sinus is that it is located where the superior sagittal sinus bifurcates as depicted in Figure 5-a.

Confluence of sinus (CoS) detection starts by locating a seed point on the superior sagittal sinus. As depicted in Figure 4, the seed point is selected on the axial slice which is 30 mm above the center of eyeballs. It is searched on the symmetry axis, and below the center of mass of the slice within a finite width, with respect to a maximum brightness criterion.

Fig. 4. Seed point search region over a T1-MRI slice for sinus map extraction

After the seed is initialized over the sagittal sinus (Figure 4-b marked with a +), mean μ and standard deviation σ values over a small window are calculated, and a 3D region growing is performed with an initial downward motion and a growing criterion of pixel intensities greater than $\mu - \sigma$. The result of segmentation by region growing produces a sinus map, as visualized in Figure 5 with a height map overlay.

Next, the segmented sinus map is analyzed using region moments of axial slices. In this study, we defined the confluence of sinus at the slice, which has the maximum variance in the left-right direction. This is performed using a covariance matrix formed by second order central moments of the sinus map over each slice: $[\mu_{20}, \mu_{11}; \mu_{11}, \mu_{02}]$. This matrix is then decomposed into its eigenvector and diagonal eigenvalue matrices using singular value decomposition. The ratio between the two eigenvalues is used to select the slice of CoS and successfully discriminates the desired slice (Z coordinate). Axial (X and Y) coordinate of CoS is calculated using the average center of mass of the sinus map over five upper slices. Figures 5-b and 5-c depict a detected CoS landmark shown with an axis bar widget.

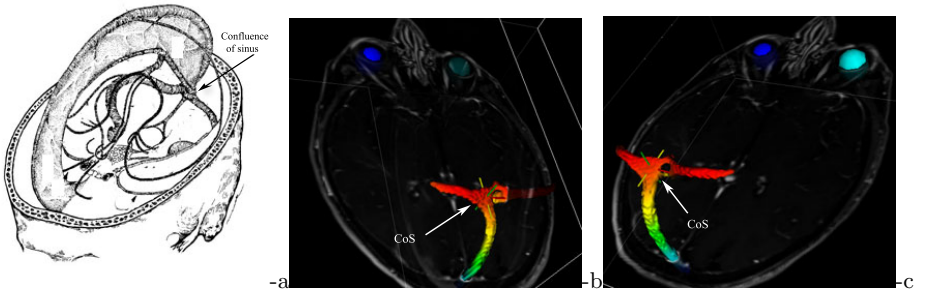

Fig. 5. (a) Cerebral venous system (figure adapted from Osborn A. Diagnostic neuroradiology. St. Louis: Mosby, 1994.) (b,c)Sinus map and CoS are shown from two different viewpoints with a height map overlaid over the surface.

2.4 Apex of Superior Sagittal Sinus

For an even sampling of landmarks over the brain, a final anatomical landmark is selected at the apex of the superior sagittal sinus. Similar to extraction of CoS, superior sagittal sinus (SSS) surface is delineated by region growing constrained by an initial upward motion. A sample SSS extracted from a contrast T1-MRI volume is shown in Figure 7. We define a plane constructed from the three anatomical landmarks: CoS, and the two eye ball centroids, as in Figure 6. This plane is called CoS-Eyeballs plane, and the point on superior sagittal sinus having a maximum distance to this plane is marked. For robustness, the center of a cloud of points with distances greater than 98% of the maximum distance is defined as the apex of superior sagittal sinus (Figure 7).

Fig. 6. CoS-Eyeballs planes from two different viewpoints

Fig. 7. Apex of Superior Sagittal Sinus is marked with axis bar widget

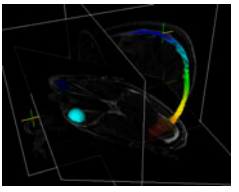

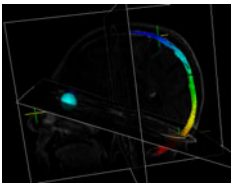

Fig. 8. All five extracted anatomical landmarks visualized together

Finally, all five anatomical extracted landmarks are visualized in Figure 8 from two different viewpoints for a sample patient contrast T1-MRI scan.

3 Registration Method

3.1 Anatomic Landmark-Based Registration

In the specific problem of registering serial MR images, a fixed reference volume, which is usually the baseline MRI scan, is to be rigidly aligned with a moving volume, which is a follow-up MRI scan. For a landmark based approach, a 3D affine transformation ($\boldsymbol{T} = \boldsymbol{A}_{3\times3}, \boldsymbol{t}_{3\times1}$) is estimated by minimizing the sum of squared distances between the extracted anatomic landmark coordinates of the fixed volume and the moving volume. $\boldsymbol{A} \in GL(3)$, the general linear group, i.e. $\boldsymbol{A}$ is an invertible 3×3 matrix. Coordinates are all in world coordinates and the centroid of the landmarks is chosen as the reference point for each MR volume. Translation component $\boldsymbol{t}$ of $\boldsymbol{T}$ is directly obtained from the difference of the centroids of the five landmarks that belong to the fixed and the moving volumes. Let $\boldsymbol{X}_f = [x_f, y_f, z_f]^T$ be a fixed landmark coordinate, $\boldsymbol{X}_m = [x_m, y_m, z_m]^T$ be its corresponding moving landmark coordinate, and $\boldsymbol{A}$ is the affine transformation between the two. Then, $\boldsymbol{A}$ can be obtained as the solution of the least squares estimation problem: $\boldsymbol{A} = \arg\min \sum_{i=1}^{n=5} ||\boldsymbol{X}_f^{\,i} - \boldsymbol{A}\,\boldsymbol{X}_m^{\,i}||^2$. After taking the derivative with respect to the unknown $\boldsymbol{A}$, equating to zero, and re-arranging the terms yields:

$$\boldsymbol{N} = \begin{bmatrix} \boldsymbol{M} & \boldsymbol{0} & \boldsymbol{0} \\ \boldsymbol{0} & \boldsymbol{M} & \boldsymbol{0} \\ \boldsymbol{0} & \boldsymbol{0} & \boldsymbol{M} \end{bmatrix}, \quad \boldsymbol{N}\,\boldsymbol{a} = \boldsymbol{b} \tag{1}$$

where $\boldsymbol{0}$ is a 3×3 all zeros matrix, and

$$\boldsymbol{M} = \begin{bmatrix} \sum_i^n x_m^2 & \sum_i^n x_m y_m & \sum_i^n x_m z_m \\ \sum_i^n y_m x_m & \sum_i^n y_m^2 & \sum_i^n y_m z_m \\ \sum_i^n z_m x_m & \sum_i^n z_m y_m & \sum_i^n z_m^2 \end{bmatrix} \tag{2}$$

and

$$\boldsymbol{b} = \left[\sum_i^n x_f x_m, \Sigma x_f y_m, \sum_i^n x_f z_m, \sum_i^n y_f x_m, \Sigma y_f y_m, \sum_i^n y_f z_m, \sum_i^n z_f x_m, \Sigma z_f y_m, \sum_i^n z_f z_m\right]^T. \tag{3}$$

The parameter vector $\boldsymbol{a} = [a_{11}, a_{12}, a_{13}, a_{21}, a_{22}, a_{23}, a_{31}, a_{32}, a_{33}]^T$ of the matrix $\boldsymbol{A}$ is calculated as $\boldsymbol{a} = \boldsymbol{N}^{-1}\boldsymbol{b}$. Final affine solution is projected to an orthogonal matrix space using a polar decomposition: $\boldsymbol{A} = \boldsymbol{Q}\,\boldsymbol{S}$, where $\boldsymbol{Q}$ is the closest possible orthogonal matrix to $\boldsymbol{A}$ in the sense of Frobenius norm, and $\boldsymbol{S}$ is a positive-definite symmetric matrix. The factor $\boldsymbol{Q}$ can be calculated using a singular value decomposition of $\boldsymbol{A} = \boldsymbol{U}\,\boldsymbol{K}\,\boldsymbol{V}^T$, where $\boldsymbol{Q} = \boldsymbol{U}\,\boldsymbol{V}^T$ [22].

3.2 Refining Surface Registration

The result of landmark based registration is further refined for an improved extensive fit of the head/scalp surface of the moving image to that of the fixed image. The binary head masks of fixed and moving volumes confined by the CoS-Eyeballs plane (Figure 6), defined in Section 2.4, are represented as the zero-level sets of two signed distance functions Φ^f and Φ^m, respectively. The sum of squared differences between the two signed distance functions:

$$E(g) = \int_{\Omega} [\Phi^f(\boldsymbol{X}) - \Phi^m(g(\boldsymbol{X}))]^2 d\boldsymbol{X} \tag{4}$$

where Ω is the domain of the image volume, is minimized to estimate a rigid transform $g(\boldsymbol{X}) = \boldsymbol{R}\,\boldsymbol{X} + \boldsymbol{t}$. The 3D rotation $\boldsymbol{R}$, and 3D translation $\boldsymbol{t}$ parameters: $g_i,\ i = 1, ..., 6$, are obtained as the steady-state solution of the ordinary differential equations:

$$\frac{\partial g_i}{\partial t} = \int_{\Omega} [\Phi^f(\boldsymbol{X}) - \Phi^m(g(\boldsymbol{X}))] < \nabla\Phi^m(g\boldsymbol{X}), \frac{\partial g(\boldsymbol{X})}{\partial g_i} > d\boldsymbol{X} \tag{5}$$

where $< \cdot, \cdot >$ denotes the Euclidean inner product in R^3, and ∇ denotes a gradient operator. We utilized the exponential coordinate representation for the 3D rotation (e.g. see [23]). The initial conditions were set to translation and rotation matrix obtained from section 3.1.

4 Results

The experiments were carried out over 9 follow-up MRI scans obtained from our clinical partner hospital (anonymized for blind review). The study was approved by the IRB of the hospital for an ongoing research project. The proposed method is validated in various ways: over synthetically transformed MRI scans, real MRI baseline and follow-up scans, a manually expert marked data set, and a data set with non-invasive fiducial landmarks attached to a patient's head. Contrast enhanced T1-weighted MRI volumes with 1mm slice thickness and axial resolution of 0.5mm are acquired from a Siemens 1.5 Tesla MR system. The proposed registration method is fully implemented in C++ environment, using Qt and VTK libraries for visualization. The parameters of the algorithm are fixed over all experiments as follows: The threshold of $\tan\beta$ is 0.40 in Section 2.1, the width of CoS seed search bounding box is 25mm, and the window size for region growing parameter calculation is 7×7 in Section 2.3.

4.1 Consistency Tests

Consistency testing method proposed by Jenkinsen et al. [21] provides a quantitative synthetic validation procedure for our method. In this test, new images are created using several pre-determined transformations with rotation and translation. All transformed images are then registered to the reference image. If the method is consistent, prescribed and calculated transformations should be the same. Performance of the proposed method is tested with a consistency dataset containing 8 contrast enhanced T1-MR and their artificially transformed MR volumes with a known transformation matrix constructed by 5 degrees of rotation about Z axis, 5 degrees of rotation about Y axis, and translated by [2,4,-2] mm in this case. Registration is carried out using anatomical landmarks described in Section 3.1, and followed by a surface based refinement procedure described in Section 3.2. In an ideal case, prescribed and calculated transformation matrices should be identical. In this study we report the Frobenius norm $\|\boldsymbol{S}\| = \sqrt{trace(\boldsymbol{S}^T * \boldsymbol{S})}$, where $\boldsymbol{S}$ is the difference of the prescribed and calculated rotation part of transformation matrices. The error in translation is interpreted as distance in milimeters.

The proposed method is compared to one of the widely adopted standard rigid registration methods based on maximization of a global mutual information criterion (MI) [17]. Observed rotation and translation errors are interpreted as mean ± standard deviation as shown in Table 1. Both methods have similar error results for rotation (less variance with the proposed method), and the proposed method is more consistent in terms of the translation. Furthermore, the proposed method takes typically 5-10 minutes of processing time on a personal computer with 3.16 GHz processor, whereas the MI method takes typically 30 minutes of processing time for our datasets. Therefore, the landmark-based method is more efficient in terms of computation times.

Table 1. Transformation error measures of consistency dataset

	Mutual Information Based	Anatomical Landmark Based with Surface Refinement
Rotation Error	0.015 ± 0.014	0.019 ± 0.008
Translation Error (mm)	1.53 ± 0.56	0.53 ± 0.20

4.2 Validation Studies on T1-MRI

Validation Studies on a Dataset with Fiducial Landmarks. For a validation study on a real MRI data, fish oil tablets are used as fiducial landmarks and 6 tablets are positioned with an unbiased sampling over the surface of the head of a patient. Two contrast enhanced T1-MRI scans are performed: the first scan in a regular patient position, and the second scan performed after the patient head is gently tilted about the axial axis. For both scans, fiducial landmarks are

segmented and a rigid transformation matrix is calculated using the method mentioned in Section 3.1. These parameters are used as the "ground truth" transformation parameters in this experiment. Fiducial landmarks are then removed from both of the volumes, and anatomical landmarks are automatically extracted, and registration is performed as described in Section 3. The two fiducially marked volumes are also aligned using the mutual information based registration algorithm. Differences between the estimated transformation parameters and the "ground truth" parameters are reported in Table 2. The parameters estimated by the proposed registration method were closer to the "ground truth" parameters than those of the mutual information based method for the fiducially marked volumes.

Table 2. Transformation error measures for fiducial landmark data. Rotation error is reported in the sense of Frobenius norm between the two rotation matrices.

Registration Method	Rotation Error	Translation Error (mm)
Landmark based	0.013	0.54
Landmark based with surface refinement	0.016	0.45
Mutual Information based	0.496	8.18

Studies on Follow-up contrast T1-MRI. In order to show the effect of the surface registration step (Section 3.2) in our algorithm, an intensity based measure, which is the sum of squared intensity differences (SSID) is utilized:

$$SSID = \int_{\Omega} [I(\boldsymbol{X}_f) - I'(\boldsymbol{T}(\boldsymbol{X}_m))]^2 \, d\Omega \tag{6}$$

where I is the fixed intensity image and I' is the registered intensity image. Follow-up MRI scans from 8 patients were registered to their baseline scans and the mean SSID results are presented in Table 3. It can be observed that adding the surface refinement process after landmark-based registration reduces the intensity match error in the registration of follow-up scans to their baseline scans, and in general improves the registration performance.

Table 3. SSID error measures over registration of T1-MRI baseline and follow-up datasets

Registration Method	Error
Landmark based	2.34E+07
Landmark based with surface refinement	2.05E+07

Validation Studies with manual expert guided registration. For comparison of our automatic landmark extraction to an expert's manual landmark extraction, one radiologist in our team manually marked 6 landmarks, which are not necessarily the computationally extracted landmarks (since for instance it is

Table 4. SSID error measure in comparison tests with expert guided manual landmarks

Registration Method	Error
Landmark based	2.12246E+07
Landmark based with surface refinement	2.29632E+07
Expert guided manual landmark based	2.34145E+07

not possible to visually mark the 3D centroid of eyeballs), in two baseline and corresponding follow-up contrast T1-MRI volumes. Registration is performed using these expert guided manual anatomical landmarks, and also using the proposed method (both with and without surface refinement step). SSID measures are given in Table 4, and as can be observed the expert guided registration produced larger errors after registration. This indicates that the consistency of manual landmark localization is lower when compared to our automatic landmark extraction algorithm.

Qualitative Results. We show sample image registration results for qualitative evaluation of the proposed method. Figure 9 shows image slices from two different patients having tumors appearing in various locations of the brain. The follow-up scan, which was performed several months later, was aligned with the

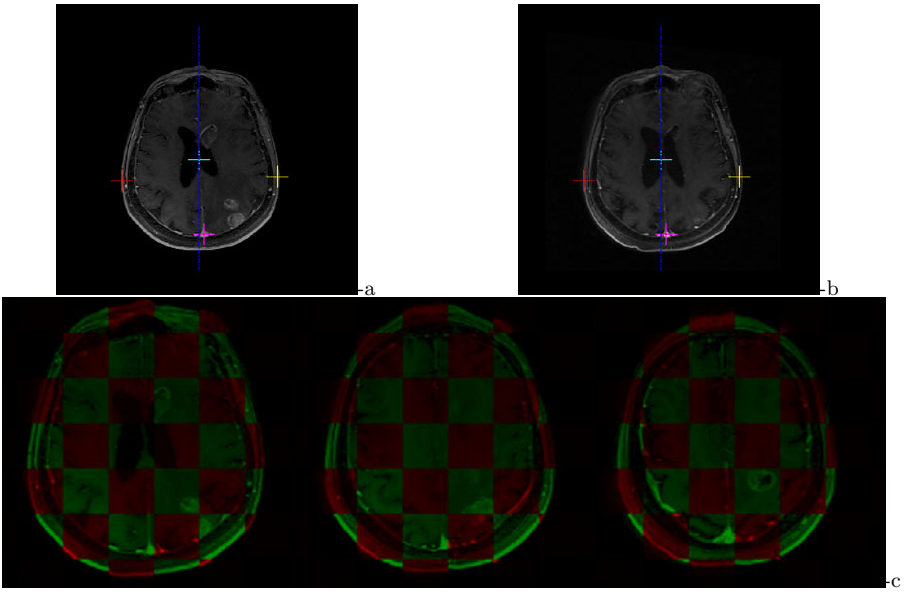

Fig. 9. Qualitative evaluation of a sample case with 3 months follow-up volume registration results: a)Baseline slice, b)Registered Follow-up slice, c)Checker board view with baseline image slices (green patches) and registered follow-up slices (red patches).

baseline scan using the proposed rigid registration method. As can be observed in the checker board view, the proposed method successfully registered the two contrast T1-MRI volumes, which are routinely used in monitoring tumor progress and response to therapy. In both cases, after treatment, the tumors regressed significantly, with reduced margins as observed in the follow-ups.

5 Conclusions and Discussions

We presented a new rigid registration method which is based on original anatomical features extracted from brain contrast-MRI scans, and a landmark-based registration refined with a surface-based registration for an improved alignment of the brain surfaces. One main application is the registration of follow-up MRI volumes in brain tumor patients, where the image intensity characteristics will vary due to tumor growth and possible different contrast characteristics depending on the scan acquisition time of the contrast enhanced MRI scans. The presented landmark-based registration method, is relatively more robust against such changes, as it is not directly based on an intensity-based optimization procedure, and is only prone to errors at the anatomic landmark extraction stage. Various validation studies demonstrated the performance of the proposed method to be as accurate as the state-of-the-art (e.g. mutual information based registration), and more efficient in terms of computation times of the algorithm, and it successfully registers contrast enhanced T1-MRI volumes. Future directions of our work includes improvement of the robustness of feature extraction, implementation of the algorithm in a multi-resolution framework, and use of the proposed method in quantification of tumor change in serial MRI sequences.

References

1. Modersitzki, J.: Numerical methods for image registration. Oxford University Press, Oxford (2004)
2. Zitova, B., Flusser, J.: Image registration methods: a survey. Image and Vision Computing 21, 977–1000 (2003)
3. Fischer, B., Modersitzki, J.: Ill-posed medicine–an introduction to image registration. Inverse Problems 24, 1–16 (2008)
4. Maintz, J., Viergever, M.: A survey of medical image registration. Medical Image Analysis 2, 1–36 (1998)
5. Angelini, E., Clatz, O., Mandonnet, E., Konukoglu, E., Capelle, L., Duffau, H.: Glioma Dynamics and Computational Models: A Review of Segmentation, Registration, and In Silico Growth Algorithms and their Clinical Applications. Current Medical Imaging Reviews 3, 176–262 (2007)
6. Patriarche, J., Erickson, B.: A Review of the Automated Detection of Change in Serial Imaging Studies of the Brain. J. Digit. Imaging 17, 158–174 (2004)
7. Ettinger, G.J., Grimson, W.E.L., Lozano-Perez, T., Wells III, W.M., White, S.J., Kikinis, R.: Automatic registration for multiple sclerosis change detection. In: IEEE Workshop on Biomedical Image Analysis, Los Alamitos, CA, pp. 297–306 (1994)

8. Chui, H., Win, L., Schultz, R., Duncan, J.S., Rangarajan, A.: A unified non-rigid feature registration method for brain mapping. Med. Image. Anal. 7(2), 113–130 (2003)
9. Davatzikos, C., Prince, J.L.: Brain image registration based on curve mapping. In: IEEE Workshop on Biomedical Image Analysis, Los Alamitos, CA, pp. 245–254 (1994)
10. Davatzikos, C., Prince, J.L., Bryan, R.N.: Image registration based on boundary mapping. IEEE Transactions on Medical Imaging 15(1), 112–115 (1996)
11. Douglas, N.G., Bruce, F.: Accurate and robust brain image alignment using boundary-based registration. Neuroimage (2009)
12. Christensen, G.E.: Inverse consistent registration with object boundary constraints. In: IEEE International Symposium on Biomedical Imaging, vol. 1, pp. 591–594 (2004)
13. Talairach, J., Tournoux, P.: Co-planar stereotaxic Atlas of the Human Brain. Thieme Medical Publishers (1988)
14. Verard, L., Allain, P., Travere, J.M., Baron, J.C., Bloyet, D.: Fully Automatic Identification of AC and PC Landmarks on Brain MRI Using Scene Analysis. IEEE Transactions on Medical Imaging 16(5), 610–616 (1997)
15. Rohr, K., Stiehl, H., Sprengel, R., Buzug, T., Weese, J., Kuhn, M.: Landmark-based elastic registration using approximating thin-plate splines. IEEE Trans. Med. Img. 20(6), 526–534 (2001)
16. Thirion, J.P.: New feature points based on geometric invariants for 3d image registration. Int. J. of Computer Vision 18(2), 121–137 (1996)
17. Viola, P.A., Wells, W.M.: Alignment by maximization of mutual information. International Journal of Computer Vision 24(2), 137–154 (1997)
18. Penney, G.P., Weese, J., Little, J.A., Desmedt, P., Hill, D.L.G., Hawkes, D.J.: A comparison of similarity measures for use in 2-D-3-D medical image registration. IEEE Trans. on Med. Imaging 17, 586–594 (1998)
19. Pluim, J., Maintz, J., Viergever, M.: Image registration by maximization of combined mutual information and gradient information. IEEE Trans. on Med. Imaging 19(8), 809–814 (2000)
20. Fitzpatrick, J.M., West, J.B., Maurer, C.R.J.: Predicting error in rigid-body point-based registration. IEEE Trans. Med. Imaging 17, 694–702 (1998)
21. Jenkinson, M., Smith, S.: A global optimisation method for robust affine registration of brain images. Med. Image. Anal. 5(2), 143–156 (2001)
22. Golub, G.H., Van Loan, C.F.: Matrix Computations. JHU Press (1996)
23. Murray, R.M., Li, Z., Sastry, S.: A Mathematical Introduction to Robotic Manipulation. CRC Press, Boca Raton (1994)